Article:

The Fretting of CoCrMo and Ti6Al4V Alloys in Modular Prostheses

A. Oladokun[a]*, M.Pettersson[b], M. Bryant[a], H. Engqvist[b] C.Persson[b], R.Hall[a], A. Neville[a]

*mn10a2o@leeds.ac.uk

[a] Institute of Functional Surfaces (iFS), School of Mechanical Engineering, University of Leeds
[b] Applied Materials Science, The Ångström Laboratory, Uppsala University

ABSTRACT

Implantation of a Total Hip Replacements (THR) is an effective intervention in the management of arthritis. Modularity at the taper junction of THR was introduced in order to improve the ease with which the surgeon could modify the length of the taper section and the overall length of the replacement. Cobalt Chromium (Co-28Cr-6Mo) and Titanium (Ti-6Al-4V) alloys are the most commonly used materials for the device. This study investigates the fretting behavior of both CoCr – CoCr and CoCr – Ti couplings and analyses their damage mechanisms. A reciprocating tribometer ball-on-plate fretting contact was instrumented with in-situ electrochemistry to characterize the damage inflicted by tribocorrosion on the two couplings. Fretting displacements amplitudes of 10, 25 and 50 μm at an initial contact pressure of 1 GPa were assessed. The results reveal larger metallic volume loss from the CoCr – CoCr alloy compared to the CoCr – Ti alloy and the open circuit potential indicates a depassivation of the protective oxide layer at displacement amplitudes > 25 μm. In conclusion, the damage mechanisms of CoCr – CoCr and CoCr – Ti fretting contacts were identified to be wear and fatigue–dominated mechanisms respectively.

Key words: Fretting, Corrosion, Orthopedics, CoCr, Ti6Al4V, Taper junction, Modularity

1. INTRODUCTION

The Total Hip Replacement (THR) has become, over the past six decades, a key intervention in providing a long term solution to the problem of arthritis[1]. Metallic materials have been used in the design of THRs since their conception in the 19th century[2]. In the 1970s, modularity was introduced to the design of THR prostheses; hence creating a ceramic – metal and/or metal – metal contact at the modular taper junction[3, 4]. The metal – metal contacts are couplings of either similar or dissimilar metallic alloys[5-7]. Cobalt chromium (CoCr) and titanium (Ti)–based alloys are the two most common biomedical materials used in THR prostheses[7]. Nonetheless, the failure of these alloys *in-vivo* as a result of tribocorrosion is widely reported in literature[3, 8]. Tribocorrosion in this context is the process whereby the interface of the metallic components at the taper junction experiences wear and corrosion[9]. The consequence of the tribocorrosion of THR implants is the release of metallic nano-particles and metallic ions into the surrounding body tissues and blood stream. The adverse reactions of these particles and ions in the body lead to the formation of pseudo-tumours, inflammation and tissue necrosis.[7, 10-12].

In the 1980s, the stiffness at the taper junction was determined to be too high and it was hypothesized that reducing it would improve the stability of the device *in-vivo*[13]. This contributed to the popularity of dissimilar metallic contacts; these were mainly CoCr heads coupled with Ti alloy stems. However, literature reveals the severe failure of some of these prostheses. The Ti stems were observed to fail by fracture and voluminous metallic particles and ion release were also observed from the modular interface of these devices[7, 13, 14]. In the early 1990s, Gilbert et al[7] examined 148 retrieved modular hip prostheses which comprised of both similar and dissimilar couplings of CoCr and Ti alloys. Using scanning electron microscopy (SEM), corrosive attack, fretting and pitting were discovered on the retrievals. For the dissimilar retrieval coupling, a Ti-Cr-Mo interfacial phase formation was also observed at the taper interface. Furthermore, the study hypothesized that high cyclic stresses led to an unstable oxide film at the taper junction which affected the type of corrosion in the region. Shortly after, Brown et al[14], measured fretting currents due to the relative motion of the alloys and concluded that limiting this relative motion could improve the resistance against tribocorrosion at the interfaces of modular prostheses. Swaminathan and Gilbert[5] is one of the most recent publications regarding the fretting corrosion of these alloys. Fretting current densities were measured at the interface of both CoCr – CoCr and CoCr – Ti implants. These were

reported to vary on the basis of the dominating fretting regime at the contact. Fretting currents were measured for both alloy couplings including the stick regime (almost zero relative motion). Although the assessment of fretting current is beyond the scope of this study, Swaminathan and Gilbert's[5] finding helps to appreciate the effect of fretting regime on the corrosion behaviour of the alloys. Furthermore, it was concluded that relative interfacial motion was dependent on the interfacial compliance of the material couplings.

In this vein, whilst Swaminathan and Gilbert's[5] approach was the varying of contact pressure of fretting contacts, the current study takes an alternative approach by assessing the fretting contact of CoCr – CoCr and CoCr – Ti through varied fretting amplitudes for a constant 1 GPa initial contact pressure. This study aims to characterise a broad range of micro-motions (10, 25 and 50 µm) and hence, fretting regimes that may arise at the taper connection due to the various contact geometries of the modular taper junction *in-vivo*.

2. EXPERIMENTAL METHODS

2.1 Metallic Alloys

To assess the fretting regime and the interaction between wear and electrochemical reactions of the two couplings CoCr – CoCr (CC) and CoCr – Ti (CT), Ø28 mm low carbon wrought cobalt chrome alloy THR heads (Co-28Cr-6Mo, Peter Brehm, Germany) were used. The plates used were Ø25 mm and 6 mm thick CoCr alloy of the same material specification as the head component. For the titanium plates, wrought titanium alloy (Ti-6Al-4V, ASTM F-136, Peter Brehm, Germany) was used. Table 1 shows the specified wt. % composition of the element constituent and mechanical properties of the two alloys.

Table 1

Chemical composition (by percentage) and mechanical properties of CoCr and Ti alloy

	Cr (%)	Mo (%)	Fe (%)	Mn (%)	Si (%)	C (%)	Ni (%)	N (%)	Co (%)	E (GPa)	v
LC CoCr	26.0-30.3	5.0-7.0	0.75 max	1.0 max	1.0 max	0.14 max	1.0 max	0.25 max	Bal.	220	0.32
	Ti	**Al**	**Fe**	**V**	**O**	**C**	**-**	**N**	**-**	**E (GPa)**	v
Ti-6Al-4V	Bal	6.15	0.2	4.19	0.143	0.005	-	0.006	-	114	0.34

2.2 Solution and Surface Preparation

Tribocorrosion tests were run in a 25 vol. % diluted foetal bovine serum solution (Sera Laboratories International Ltd., West Sussex, UK) with phosphate buffered saline (PBS) dissolved in de-ionized water as the balance (Sigma-Aldrich, Co., St. Louis, USA) and 0.03 vol. % sodium azide (GBioscienics, St. Louis, USA). Samples were rinsed thoroughly in de-ionized water and the plates were immersed in the serum solution for 1 h prior to the test. This process was found, during this study, to bring the initial potential of the tribo-couples closer together hence, suggesting the formation a uniform proteinaceous film on the surface of the plates (although, this method wasn't as effective on CT tribocouples). All surfaces were polished to an average surface roughness of $R_a \approx 20$ nm by using a diamond suspension of 3μm as the final polishing stage.

2.3   Electrode and Tribocorrosion Arrangement

Fretting displacements were applied via the ball onto the plate component through the electromechanical actuator of the fretting rig. The tangential force (F_t) was measured through a fitted cylindrical force transducer (Kistler, USA); positioned axially to the middle of the actuator and the CoCr ball (Figure 1). The reciprocating motion of the ball sample relative to the plate was measured by a fiber optic sensor fitted to the axially positioned actuator (Figure 1). The plates were fitted into a polymer bath and plastic screws were used to fasten a concentric plastic fitted with two concentric O-rings onto the plate and the polymer bath; hence fixing both parts tightly together to ensure a water tight seal. The plate was loaded against the ball sample in the vertical direction.

The electrical connection required to assess electrochemistry was taking from the CoCr ball in each instance. This is identified as the working electrode (WE) in Figure 1. The standard 3-electrode electrochemical cell comprises of the reference electrode (RE), the counter electrode (CE) and the WE. The combined electrode (Redox/ORP electrode, Thermo Fisher Scientific Inc., MA, USA) that was used in this study (see Figure 1) consists of Ag/AgCl (+0.196V vs. Standard Hydrogen Electrode) as the RE and a platinum wire as the CE. The WE were the CC and CT tribo-couples.

The test conditions for this study are shown in Table 2. Whilst Zhang et al[15], using finite element analysis reported contact pressures of around 68 MPa for the modular taper junction of a full component assembly. The use of a ball-on-plate configuration in this study was to assess the contact mechanics and damaged mechanism of a single point contact for CoCr and Ti alloys. This is because the complex geometry of the modular junction is such that, whilst slip occurs on one section of the taper contact, a stick may occur on the other. Therefore, previous tribocorrosion studies have employed relatively high contact pressures ranging from 0.87 – 1.3 GPa in order to encourage various fretting regimes at the contact. These are namely: stick, partial slip and gross slip fretting regimes[4, 5, 16]. This study for similar reasons assessed the fretting behavior of the CoCr and Ti tribo-couples at an initial Hertzian contact pressure of 1GPa. The corresponding fretting displacement amplitudes imposed on the tribo-couples are therefore, 10, 25 and 50 µm which would generate at least two of the three fretting regimes.

In this study, displacement amplitude of 25 μm would correspond to 50 μm of slip assuming a 100% slip – displacement ratio. Literature reports micro-motions at the modular taper measuring an average of 45 μm in length[17]. Therefore, this study assesses displacement amplitudes both below (10 μm) and above (50 μm) the corresponding displacement amplitude of ~25 μm (~50 μm in length).

The evolution of corrosion as a function of fretting was monitored by integrating a 3-electrode electrochemical cell into the test apparatus in order to attain an in-situ corrosion measurement. The open circuit potential (OCP) also known as free corrosion potential of each tribo-couple was recorded throughout the tribocorrosion test at a frequency of 1 point per second (Hz). The potentiostat used for the OCP measurement was the PGSTAT101, Metrohm Autolab B.V., Utretch, Netherlands. The tribocorrosion test protocol follows the order: 1.) a pre-test immersion stage where the plate surface is exposed to serum for ~1hr; 2.) the contact is loaded for 1100 s and OCP is measured at a data acquisition rate of 1 point per seconds from this point and throughout the test; 3.) the contact is fretted for 6000 s at frequency of 1 Hz; 4.) the potential is left to recover for 1000 s.
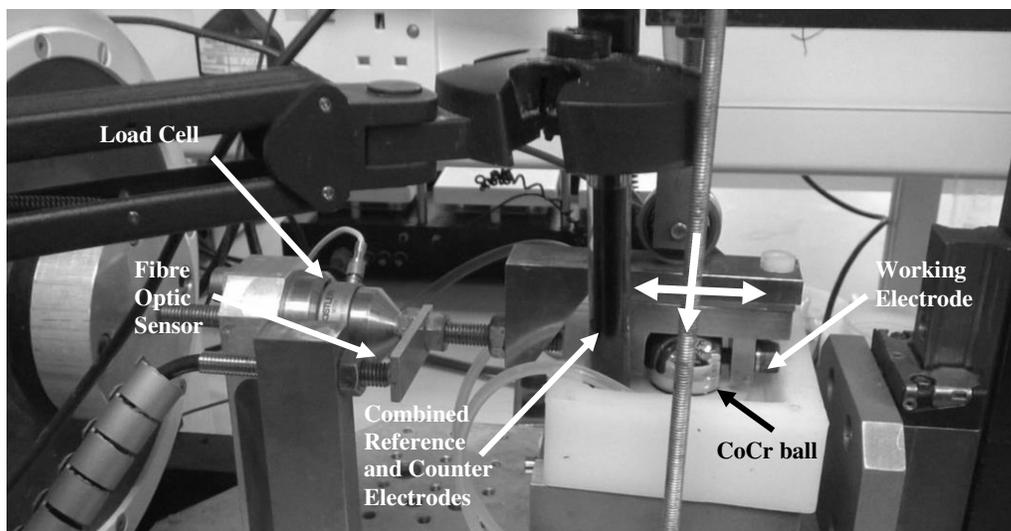

Figure 1 – Ball-on-plate arrangement in the fretting rig. The arrows above the

ball are indicating the direction of the moving component and axis of applied load.

2.4   Surface Analysis

The volume of material removed from both ball and plate components due to wear and corrosion were evaluated using vertical scanning interferometry (VSI – NPFLEX 3D Optical Profiler, Bruker Corporations). The image obtained from the scan was filtered using the "terms removal" function. This helped reduce the influence of surface form on the measured volume loss data. More so, the wear region was masked out in order to reduce the effect that irregularities on the sample surface might have on the volume loss results.

The samples were wiped thoroughly without the use of chemicals prior to interferometry. This was done to preserve any tribofilms at the contact area. Optical microscopy (Leica DM 6000 M, Germany) was used to capture the wear scar of the plate components. The scanning electron microscope (SEM) used in this study was an SEM attached to a focused ion beam (FIB). The SEM/FIB was the Nova 200 Nanolab dual beam SEM/FIB fitted with a Kleindiek micromanipulator. The machine was used to obtain close-up micrograph (~1000 Mag) of CoCr and Ti flats at 50 µm fretting displacement.

Table 2

Test parameters of CoCr – CoCr and CoCr – Ti fretting couples

Material Couple		
CC =	CoCr – Ball	CoCr – Plate
CT =	CoCr – Ball	Ti6Al4V – Plate
Fretting Parameters		
Displacement Amplitude (δ_d)		10, 25 and 50 µm
Initial Hertzian Contact Pressure (P_{max})		1 GPa
Frequency		1 Hz
Number of Cycles		6000
Corresponding Normal load (F_N)		CC (50 N) CT (120 N)
Surrounding fluid		25% diluted FBS, PBS Balance, 0.03% SA, 12 ml fluid volume, temperature of 37ºC
Repetitions (n)		2

3. RESULTS AND DISCUSSION

3.1 Tribological Evaluation

The fretting regimes characterized in this study were obtained from the plots of F_t vs. δ_d where (F_t) corresponds to the tangential force measured for a lateral displacement and (δ_d) corresponds to the fretting amplitude. Figure 2 shows a schematic representation of the three fretting regimes observed in this study. The stick regime is characterized by a tightly closed loop while the mixed regime known to some as "Partial slip" and to others as "stick – slip" is represented by different forms of quasi-rectangular shapes with pointed corners. It is worth noting that the "mixed regime" in literature follows two different interpretations: the first means partial slip and partial sticking occurs at a fretting contact simultaneously[18]; the second says that the regime at a fretting contact changes from one to another during an ongoing fretting study[19]. This study refers to the interpretation of the former. Unlike the mixed (partial slip) regime, the fretting loop of gross slip regime is generally a rectangular-like shape[18-21]. The area enclosed in fretting loops (shaded in grey) corresponds to the dissipated energy (E_d) from the fretting interactions at the contact. The width of the fretting loop represents the relative slip 'S' (denoted as δ_s) measured from the contact. The width from one corner of the loop to the other represents the total displacement 'D'. The ratio (S/D) is significant for characterizing both fretting regime and damage mechanism of a fretting contact[19, 22].

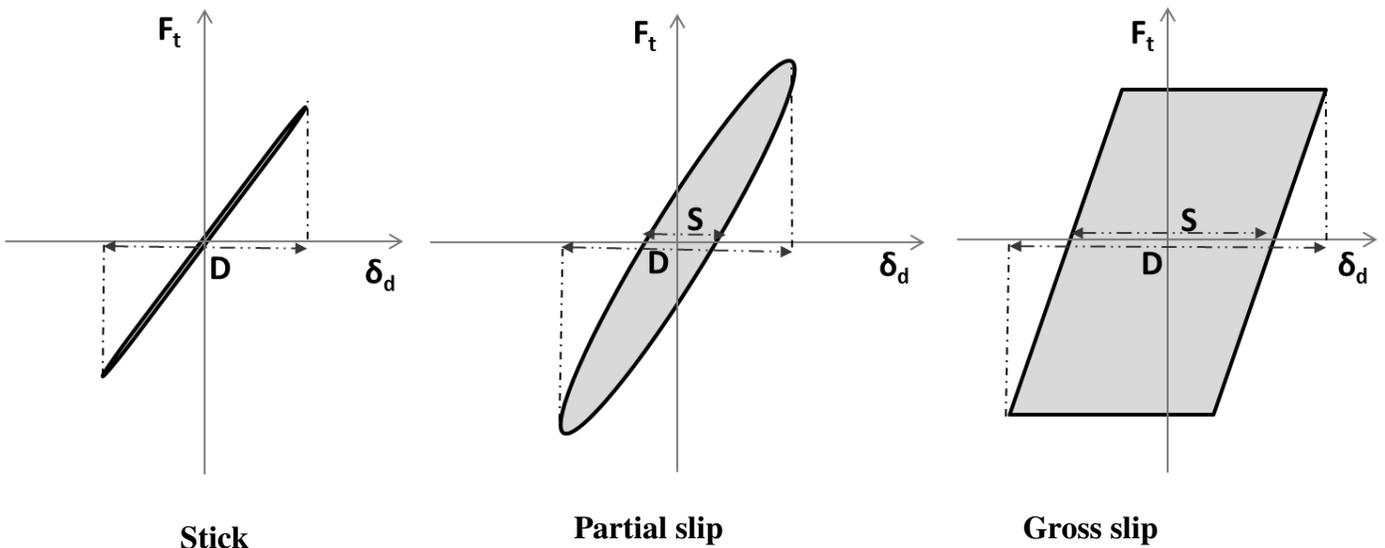**Stick**   **Partial slip**   **Gross slip**

Figure 2 – Schematic diagram of the three fretting regimes. 'S' denotes the relative sliding at the contact and 'D' denotes the displacement amplitude.

Vingsbo and Soderberg[20] researched further into fretting regimes by expressing the contact mechanics and damage mechanisms associated with each regime. The stick regime is mainly characterized by minimal wear as a result of almost zero measured relative motion. The fretting contact is entirely elastic deformation dominated resulting in possible crack nucleation of the materials. The mixed regime however, accommodates some sliding along with high elastic deformation hence making the effect of fatigue more predominant in this regime. The gross slip regime is a highly energy dissipative regime with almost zero measured sticking occurring at the fully sliding contact; the surface degradation is manifested as debris formation[19, 22, 23]. Theoretically, $E_d = f (F_t, \delta_s)$, this is equivalent to the interfacial work done to shear the contact interface[19]. When considering this two parameters that make up the dissipated energy, the contact compliance at the tribo-couple interface is the determinant by which one of the two parameters (either F_t or δ_s) will dominate the evolution of this dissipated energy[20]. The higher the elastic contact compliance of a tribo-couple, the higher the required frictional force (F_t) to overcome before slip commences at the contact[22].

Figure 3 shows the fretting loops obtained for CC and CT. Both tribo-couples at $\delta_d = 10$ µm reveal a stick fretting regime with maximum S/D ≈ 0.1. The expected minimal damage is reflected in the total volume loss measured from the ball and plate components as shown in Figure 4. When comparing $\delta_d = 10$ to $\delta_d = 25$ µm for CC, Figure 3a and c shows a transition from stick regime into a gross slip regime for the CC tribo-couple and a transition from stick regime into a partial slip regime for the CT tribo-couple (Figure 3b and d) respectively. The total volume of materials removed from the contact is substantially increased for CC and comparably larger than that of CT. The difference in transition between the two tribo-couples reveals a significant difference in the contact compliance of CC and CT. Figure 3 shows that the friction force measured at the CT contact increased significantly (14 N to 30 N) from $\delta_d = 10$ to $\delta_d = 25$ µm whereas, the slip-displacement ratio increased ~8 times for the CC tribo-couple with little change in F_t as shown in Figure 4a. This illustrates the relative ease of CoCr to slide against itself than against the softer and more ductile Ti alloy. This finding can be explained using the arrows on Figure 3. Figure 3c and e; both show a horizontal arrow to depict full slip behavior across the stroke length while a constant friction force is measured. On the other hand, the arrow shown on Figure 3f depicts an increasing tangential force relative to the slip; hence the slope of the non-horizontal line corresponds to a change in the stiffness (change in force per displacement) at the contact. A change in the contact stiffness during sliding

at the contact further highlights the high elastic compliance of the CT hence a higher tendency of fatigue failure in CT[24]. Fouvry et al[22] discussed the typical behavior of ductile materials changing in their ductility due to phase transformation induced by cyclic plastic deformation. Although, it is beyond the scope of this study to identify possible phase transformation that might have occurred due to fretting, this study identifies the prerequisite characteristic for such fatigue damage mechanism. This is mainly high friction force that leads to highly localized stresses which thereby aids the initiation cracks at the dominant mixed fretting regime[20, 24]. When observing the optical microscope images of figure 5 for both CC and CT at the three displacement amplitudes, it is observable that the fretting wear debris on the CC plates (Figure 5 a, c and e) increases with each higher displacement amplitude. On the other hand, with CT (Figure 5 b, d and f), fretting wear debris isn't increasingly observed; rather, fatigue damage is identifies as it is visible at the localized regions of highest stresses as expected[18-20]. Further increase in the displacement amplitude reveal a mixture of both fatigue localized damage and fretting wear. SEM micrographs in Figure 6a and b depicts a close up image of both CC and CT fretting mechanisms at 50 µm displacement amplitude. This study therefore identifies CC to have a wear dominated damage mechanism through material delamination and relatively high volume loss at the fretting contact. And CT – a fatigue dominated damage mechanism through material detachment and pit formation along with suppressed volume loss at the contact[24].
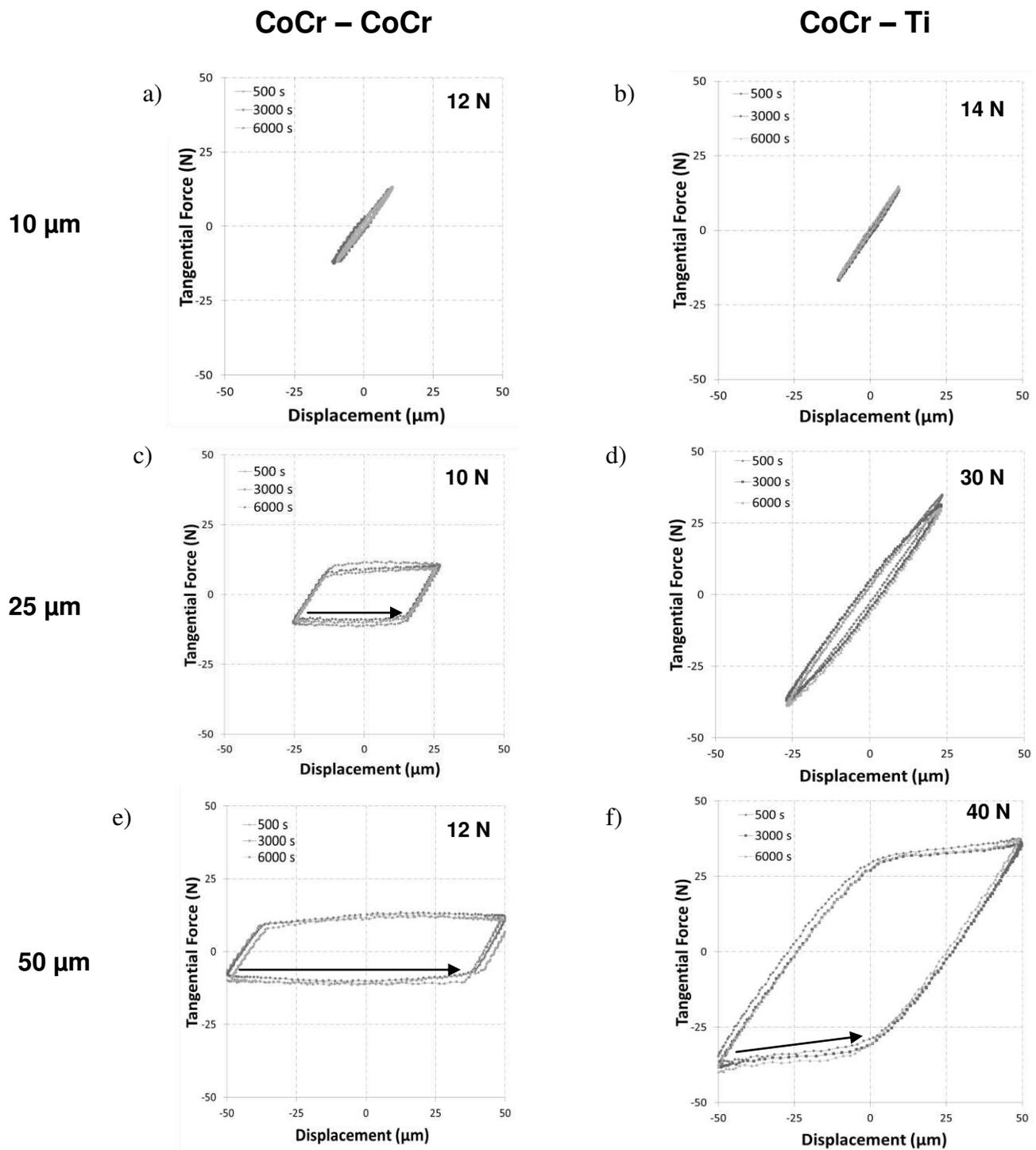
Figure 3 – Fretting Regimes for a) CoCr – CoCr and b) CoCr – Ti tribo-couples. Arrows indicate the slope of the displacement across the slip region of the stroke length. The average tangential force is indicated at the top right corner of each plot.
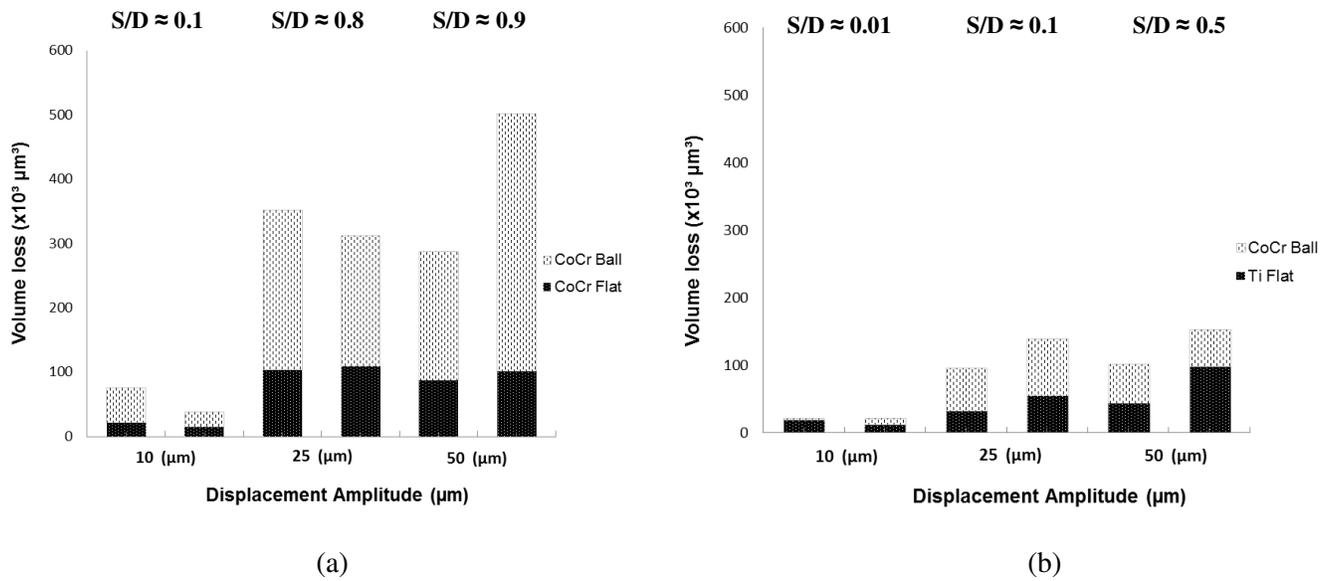
Figure 4 – Final mass loss after 6000 cycles of fretting for a) CC and b) CT tribo-couples n = 2. The sliding – displacement (S/D) ratio for each displacement amplitude is indicated above.

CoCr – CoCr

CoCr – Ti

a.) Stick Contact

10 μm

Partial–slip

200μm

b.) Stick Contact

200μm

c.) Third body

25 μm

200μm

d.) Fatigue damage

200μm

e.) Third body

50 μm

200μm

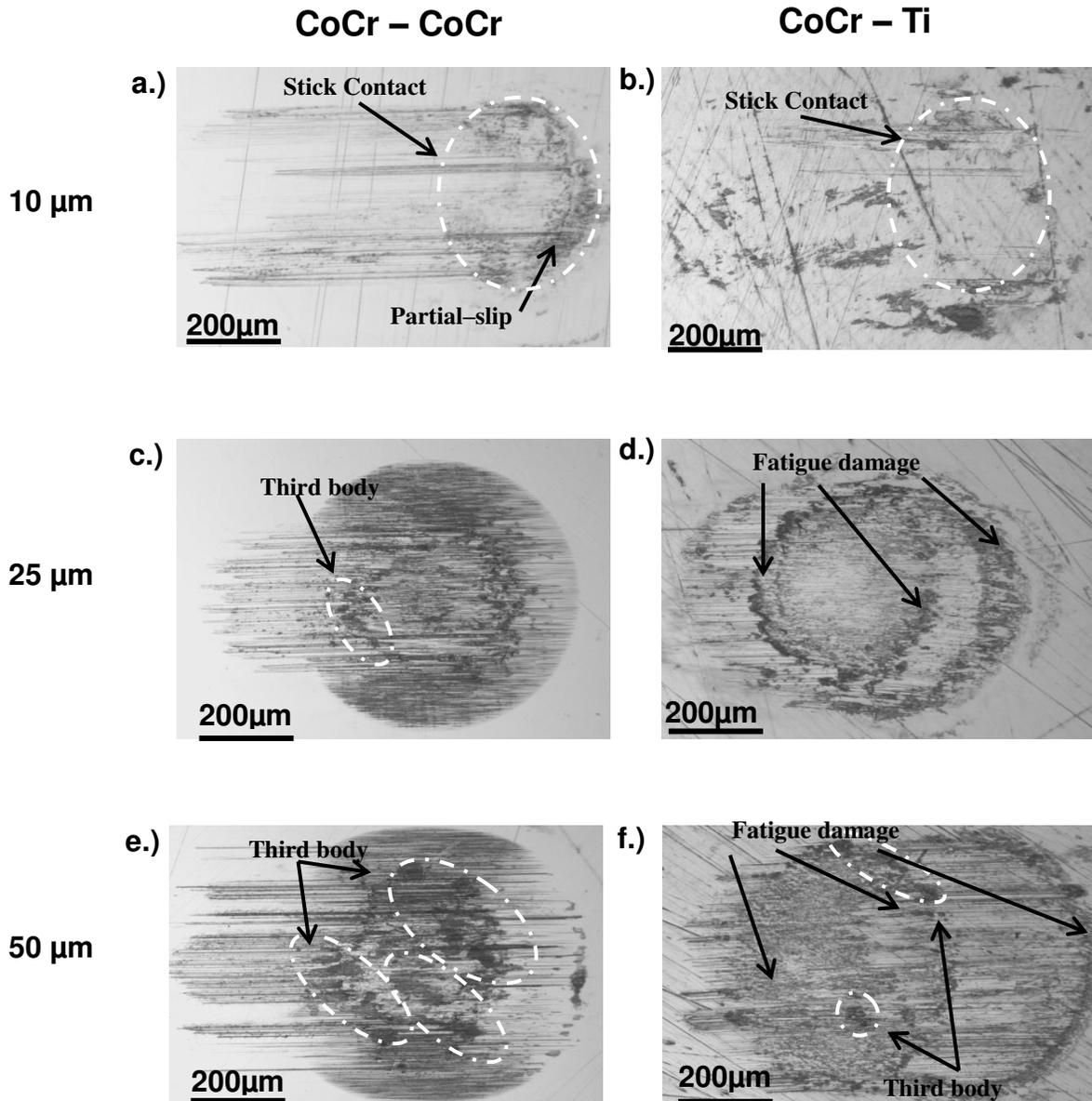f.) Fatigue damage

Third body

200μm

Figure 5 – Fretting wear scar of CoCr plate of CC and Ti plate of CT obtained through optical microscope respectively. The dotted region of CC – 10 and CT – 10 μm represents the only concerned region. Scratches seen outside this region were incurred as a result of the fretting machine stabilizing.
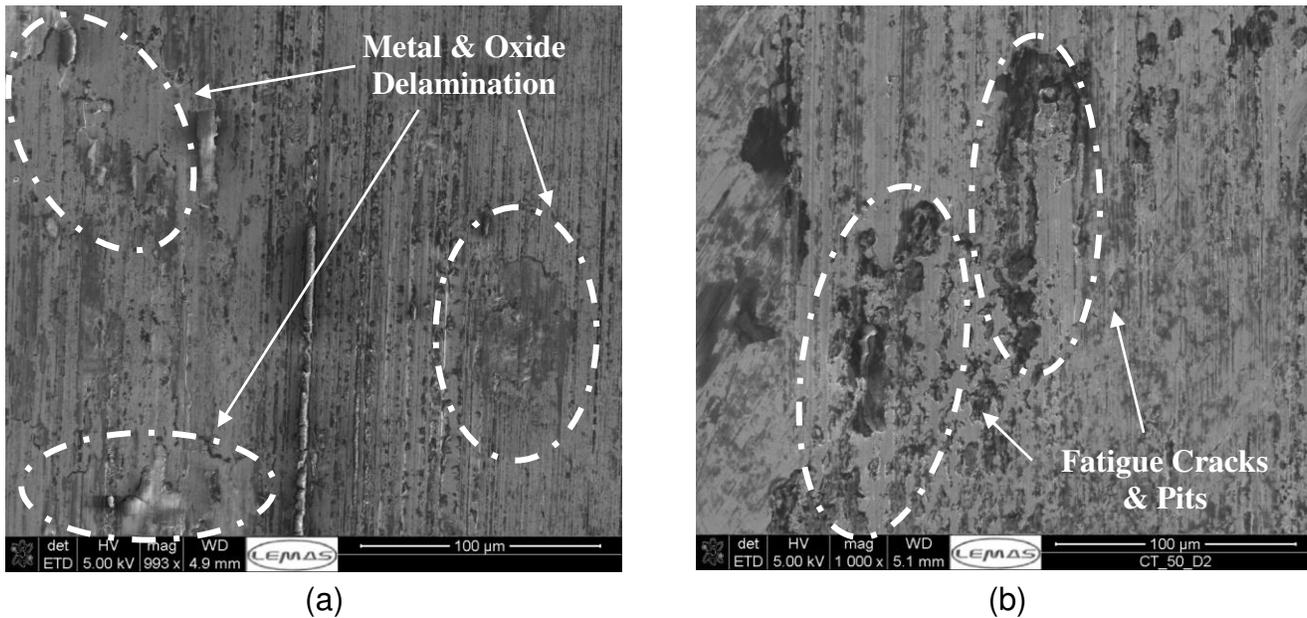
Figure 6 – SEM image of wear scar for a) CC – 50 μm (Figure 5e) and b) CT – 50 μm (Figure 5f) tribo-couples.
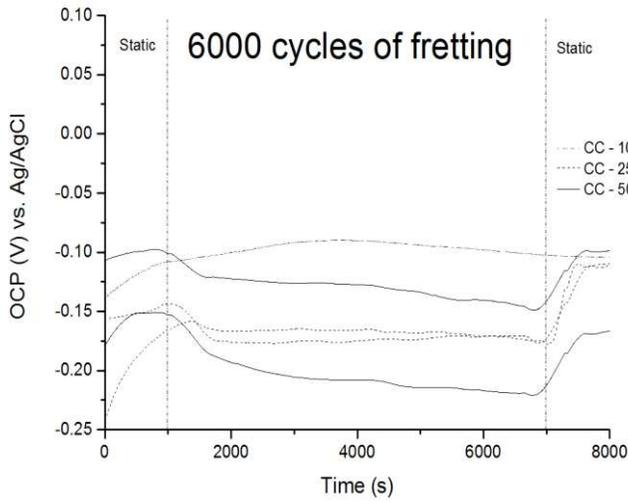
3.2   Electrochemical Evaluation

CoCr and Ti alloys are both passive alloys that spontaneously form a protective oxide layer[25, 26]. Micro-motion at the fretting contact of modular tapers can however lead to the removal of the oxide layer; hence the depassivation of the alloy[4, 5, 7, 21]. This leaves the alloy exposed to electro–active species such as chloride ions, sulphate ions and complexes in the body fluid which can accelerate the dissolution of the metallic alloy *in-vivo*[27-29]. OCP is a semi-quantitative technique that enables the process of corrosion to be partially assessed[30-32]. Once the passive metal is depassivated, it behaves as an active metal due to the formation of a temporary anodic site at the contact. This is observed as a drop in potential when monitoring OCP in tribo-corrosion tests. A gradual increase in the OCP corresponds to an ennoblement (that is, a buildup of oxide) at the interface[33]. On the other hand, a recovery from depassivation is known as repassivation – a relatively sharp increase in OCP. The OCP curves observed in Figure 7 all have various starting potential because unlike potentio-static tests where the metallic surface is forced to the same potential, these tests were conducted without such electrochemical alterations of the contact.

From Figure 7, it is observable that the CC – 10 and CT – 10 (the two stick regime tribo-couples) experienced an ennoblement throughout the fretting process. Although the buildup of an oxide is a protective feature against corrosion, hence is expected to reduce the rate of corrosion, the presence of cracks or crevices at the contact may however prove otherwise. Whilst a ball on plate configuration may not provide the opportunity for crevice formation, crevices can form in the assembly of the modular taper junctions and hence induce crevice corrosion[7]. The male taper is usually threaded and locked into the female head bore. Crevices are formed both in the gap between the threads and the separation between the male and female taper. Crevice corrosion may therefore occur in this region however, it is not initiated until fluid ingresses into the crevices – this process can be accelerated by mechanical wear. It is therefore worth mentioning that a stick fretting regime of the taper junction *in-vivo* can encourage a mechanically enhanced crevice corrosion which is a type of localized corrosion[30]; the contact becomes starved of oxygen and as a result, electro-active species, especially chloride ions migrate to the crevice and cause the environment to become increasingly acidic[6, 29, 30].
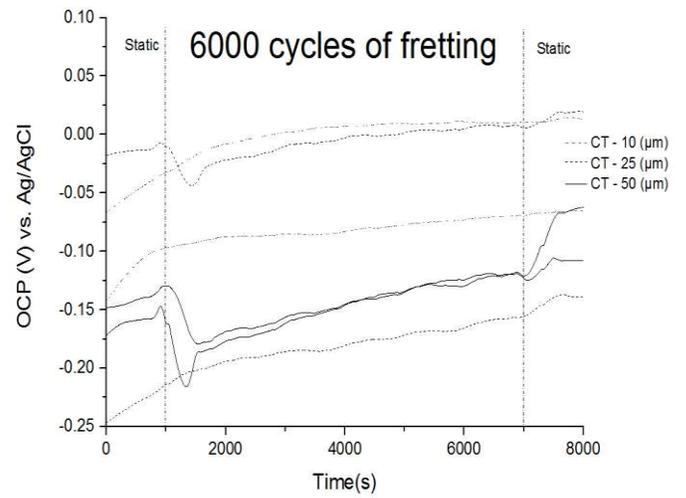
As soon as the fretting commences in Figure 7, a drop in potential can be observed for both CC and CT tribo-couples at $\delta_d \geq 25$ µm. This signifies a depassivation of the material, most likely due to removal of the oxide layer. Interestingly, the OCP plot of CC $\delta_d \geq 25$ µm differed from that of CT. At the commencement of sliding, the shift in OCP for the CC tribo-couple was observed to either remain constant as in CC – 25 or decrease gradually as in CC – 50 until the fretting ceased and repassivation occurred. On the other hand, for the CT – 25, a quick repassivation is observed almost instantly after the initial potential drop, followed by a steady ennoblement (the ennoblement for the second repeat isn't as visible due to the potential starting relatively low from start of the test). Although the drop for CT – 50 was much sharper, a gradual ennoblement at the contact persists until the fretting ceased which was similar to the behavior of CT – 25. The difference in the CC and CT behavior may have three reasons:

- The presence of a third body at the CC contact encourages an abrasive mechanism which kept the potential either constant or decreasing and inhibits the formation of new layers of protective oxide[34].

- Hanawa et al[35] reported a faster rate of titanium alloy repassivation than CoCr alloy. This suggests that Ti may be electrochemically dominant in the CT tribo-couple. For this reason, Ti alloy may be repassivating whilst the fretting persists. However, this suggestion is contrary to Swaminathan and Gilbert's[5] whose postulation was that CoCr alloy is the dominant of the two tribo-couples both mechanically and electrochemically.

- Lastly, as the CT fretting contact is a partial slip regime, the micro seconds required for repassivation to occur at the interface makes the repassivation of the Ti alloy more likely to occur. This is due to the CoCr ball moving slower as a result of the partial slip regime whereas, for the CC fretting contact, the CoCr ball is moving faster due to the gross slip fretting regime.

Whilst it was established that the potential drop from the OCP curve signifies a removal of the protective oxides, the specific damage mechanisms in the contact are not identified by the OCP although they are identified and discussed through surface analytical techniques. The delamination of oxide layers and metallic particles from the CC tribo-couple (Figure 5c and e) may lead to the acceleration of metallic ion dissolution at the exposed (anodic) region *in-vivo*[33]. However, for the CT tribo-couples (Figure 5d and f), possible surface cracks are closely observed in Figure 6b. This form of damage to the surface makes the alloy strongly susceptible to localized corrosion and hence, a mechanically assisted corrosion mechanism[6, 13]. The formation of cracks at the surface of these alloys can significantly reduce the fatigue life of the components *in–vivo*[20]. Therefore, it can be deduced that although a fatigue failure dominated fretting contact may not generate voluminous wear and corrosion products, it proves to be more susceptible to severe failure mechanisms such as fracture[24]. This could be a reason why the titanium components in hip implants have been shown to fail through fracture *in-vivo*[3, 36, 37].

(a)   (b)

Figure 7 – OCP Response as a function of time for a) CC and b) CT tribo-couples n = 2. The line prior to and after the fretting represents a static phase where the contact is loaded. The CC – 10 repeats are superimposed onto each other and the potential drop of CT – 25 repeat did not occur due to the potential starting much lower compared to the first however the same repassivation pattern is observed.

4. CONCLUSIONS

- The contact compliance for CoCr – Ti tribo-couple was found to be much higher than the CoCr – CoCr contact when the effect of friction force is compared with slip – displacement ratio; this strongly influenced the motion at the tribo-couples interfaces.

- The corresponding behaviour at the fretting contact of CoCr – CoCr was therefore a wear–dominated mechanism and fatigue–dominated mechanism for CoCr – Ti tribo-couple.

- OCP plots reveal an ennoblement of the contact for both tribo-couples at the stick regime and a depassivation of the oxides at $\delta_d \geq 25\mu$m.

- Optical microscope images reveal delaminated material and possible corrosion product on the CoCr – CoCr contact. Cracks and pits were observed at the CoCr – Ti worn area and verified with the SEM.

- It was observed that whilst CoCr – CoCr interface may suffer dissolution of metallic ions through active mechanically depassivated regions; CoCr – Ti surface is highly susceptible to various forms of localized corrosion likely due the formation of cracks at the surface.

5. REFERENCES

1.   D.Dowson, V.W., *Introduction to the Biomechanics of Joints and Joint Replacements*. Vol. 1. 1981, United Kingdom: Wiley-Blackwell.

2.   Knight, S.R., Randeep Aujla, and Satya Prasad Biswas, *Total Hip Arthroplasty-over 100 years of operative history*. Orthopedic reviews, 2011. **3**(2).

3.   Grupp, T.M., Thomas Weik, Wilhelm Bloemer, and Hanns-Peter Knaebel *Modular titanium alloy neck adapter failures in hip replacement - failure mode analysis and influence of implant material*. BMC musculoskeletal disorders 11, 2010. **1**(3).

4.   Baxmann, M.J., S. Y. Schilling, C. Blomer, W. Grupp, T. M. Morlock, M. M., *The influence of contact conditions and micromotions on the fretting behavior of modular titanium alloy taper connections*. Med Eng Phys, 2013. **35**(5): p. 676-83; discussion 676.

5.   Swaminathan, V., and Jeremy L. Gilbert, *Fretting corrosion of CoCrMo and Ti6Al4V interfaces*. Biomaterials, 2012. **33**(22): p. 5487-5503.

6.   Gilbert, J.L., M. Mehta, and B. Pinder, *Fretting crevice corrosion of stainless steel stem-CoCr femoral head connections: comparisons of materials, initial moisture, and offset length*. J Biomed Mater Res B Appl Biomater, 2009. **88**(1): p. 162-73.

7.   Gilbert, J.L., Christine A. Buckley, and Joshua J. Jacobs., *In vivo corrosion of modular hip prosthesis components in mixed and similar metal combinations. The effect of crevice, stress, motion, and alloy coupling*. Journal of biomedical materials research, 1993. **27**(no. 12): p. 1533-1544.

8.   Kurtz, S., Kevin Ong, Edmund Lau, Fionna Mowat, and Michael Halpern, *Projections of primary and revision hip and knee arthroplasty in the United States from 2005 to 2030*. The Journal of Bone & Joint Surgery 2007. **89**(4): p. 780-785.

9.   Cook, S.D., Robert L. Barrack, Gregory C. Baffes, Alastair JT Clemow, Paul Serekian, Nick Dong, and Mark A. Kester, *Wear and corrosion of modular interfaces in total hip replacements*. Clinical orthopaedics and related research 1994. **298**: p. 80-88.

10.   John Cooper, H., et al., *Corrosion at the Head-Neck Taper as a Cause for Adverse Local Tissue Reactions After Total Hip Arthroplasty*. The Journal of Bone and Joint Surgery (American), 2012. **94**(18).

11.   Gill, I.P.S., J. Webb, K. Sloan, and R. J. Beaver, *Corrosion at the neck-stem junction as a cause of metal ion release and pseudotumour formation*. Journal of Bone & Joint Surgery, 2012. **British Volume 94**(no. 7): p. 895-900.

12.   Skendzel, J.G., J.D. Blaha, and A.G. Urquhart, *Total hip arthroplasty modular neck failure*. J Arthroplasty, 2011. **26**(2): p. 338 e1-4.

13.   A. J. Wassef, T.P.S., *Femoral taperosis: AN ACCIDENT WAITING TO HAPPEN*. Bone Joint J, 2013. **95-B**(Supple A:3–6).

14. Brown, S.A., C. A. C. Flemming, J. S. Kawalec, H. E. Placko, C. Vassaux, K. Merritt, J. H. Payer, *Fretting Corrosion Accelerates Crevice Corrosion of Modular Hip Tapers.* Journal of Applied Biomaterials, 1995. **6**(1): p. 19-26.

15. Zhang, T., N. M. Harrison, P. F. McDonnell, P. E. McHugh, and S. B. Leen, *A finite element methodology for wear–fatigue analysis for modular hip implants.* Tribology International, 2013. **65**: p. 113-127.

16. Barril, S., S. Mischler, and D. Landolt, *Influence of fretting regimes on the tribocorrosion behaviour of Ti6Al4V in 0.9 wt.% sodium chloride solution.* Wear, 2004. **256**(9): p. 963-972.

17. Viceconti, M., Massimiliano Baleani, Stefano Squarzoni, and Aldo Tonil. , *Fretting wear in a modular neck hip prosthesis.* Journal of biomedical materials research, 1997. **35**(2): p. 207-216.

18. Vingsbo, O., and Joakim Schön, *Gross slip criteria in fretting.* Wear, 1993. **162**: p. 347-356.

19. Fouvry, S., Philippe Kapsa, and Leo Vincent, *Quantification of fretting damage.* Wear, 1996. **200**(1): p. 186-205.

20. O. Vingsbo, S.S., *On fretting maps.* Wear, 1988. **126**: p. 131–147.

21. Duisabeau, L., P. Combrade, and B. Forest, *Environmental effect on fretting of metallic materials for orthopaedic implants.* Wear, 2004. **256**(7-8): p. 805-816.

22. Fouvry, S., Ph Kapsa, and L. Vincent., *Analysis of sliding behaviour for fretting loadings: determination of transition criteria.* Wear, 1995. **185**(1): p. 35-46.

23. Lgried, M., T. Liskiewicz, and A. Neville, *Electrochemical investigation of corrosion and wear interactions under fretting conditions.* Wear, 2012. **282**: p. 52-58.

24. Mutoh, Y., *Mechanisms of fretting fatigue.* JSME international journal Series A mechanics and material engineering, 1995. **38**(4): p. 405-415.

25. Goldberg JR, G.J., *Electrochemical Response of Cocrmo to High-Speed Fracture of Its Metal Oxide Using an Electrochemical Scratch Test Method. .* John Wiley & Sons, 1997: p. 421-431.

26. Revie, R.W., *Thermodynamics: corrosion tendency and electrode potentials, Corrosion and corrosion control.* 2000: John Wiley and Sons, New York.

27. Hiromoto, S., and S. Mischler, *The influence of proteins on the fretting–corrosion behaviour of a Ti6Al4V alloy.* Wear, 2006. **261**(9): p. 1002-1011.

28. Mischler, S., S. Debaud, and D. Landolt, *Wear-Accelerated Corrosion of Passive Metals in Tribocorrosion Systems.* Journal of the Electrochemical Society, 1998. **145**(3): p. 750-758.

29. Tritschler, B., Bernard Forest, and Jean Rieu., *Fretting corrosion of materials for orthopaedic implants: a study of a metal/polymer contact in an artificial physiological medium.* Tribology international, 1999. **32**(no. 10).

30. Bryant, M., Xinming Hu, Richard Farrar, Ken Brummitt, Robert Freeman, and Anne Neville, *Crevice corrosion of biomedical alloys: A novel method of assessing the effects of bone cement*

and its chemistry. Journal of Biomedical Materials Research Part B: Applied Biomaterials, 2013. **101**(5): p. 792-803.

31. Y.Yan., *Corrosion and Tribo-corrosion behaviour of metallic orthopaedic implant material*. 2006, University of Leeds.

32. Hesketh, J., *Tribocorrosion of Total Hip Replacements*, in *School of Mechanical Engineering*. 2012, University of Leeds.

33. Bryant, M., R. Farrar, K. Brummitt, R. Freeman, and A. Neville, *Fretting corrosion of fully cemented polished collarless tapered stems: The influence of PMMA bone cement.* Wear, 2013. **301**(1): p. 290-299.

34. Waterhouse, R.B., *Fretting wear.* Wear 1984. **100**(1): p. 107-118.

35. Hanawa, T., *Metal ion release from metal implants.* Materials Science and Engineering: C, 2004. **24**(6-8): p. 745-752.

36. Jauch, S.Y., G. Huber, E. Hoenig, M. Baxmann, T. M. Grupp, and M. M. Morlock, *Influence of material coupling and assembly condition on the magnitude of micromotion at the stem–neck interface of a modular hip endoprosthesis.* Journal of biomechanics, 2011. **44**(9): p. 1747-1751.

37. Jauch, S.Y., et al., *Design parameters and the material coupling are decisive for the micromotion magnitude at the stem-neck interface of bi-modular hip implants.* Med Eng Phys, 2013.